Permanent magnet based dipole magnets for next generation light sources

Takahiro Watanabe,[1,2,*] Tsutomu Taniuchi,[1] Shiro Takano,[1,2]
Tsuyoshi Aoki,[1] and Kenji Fukami[1,2]

[1]*Japan Synchrotron Radiation Research Institute (JASRI), 1-1-1 Kouto, Sayo, Hyogo 679-5198, Japan*
[2]*RIKEN SPring-8 Center (RSC), 1-1-1 Kouto, Sayo, Hyogo 679-5148, Japan*

(Received 26 January 2017; published 31 July 2017)

We have developed permanent magnet based dipole magnets for the next generation light sources. Permanent magnets are advantageous over electromagnets in that they consume less power, are physically more compact, and there is a less risk of power supply failure. However, experience with electromagnets and permanent magnets in the field of accelerators shows that there are still challenges to replacing main magnets of accelerators for light sources with permanent magnets. These include the adjustability of the magnetic field, the temperature dependence of permanent magnets, and the issue of demagnetization. In this paper, we present a design for magnets for future light sources, supported by experimental and numerical results.

DOI: 10.1103/PhysRevAccelBeams.20.072401

I. INTRODUCTION

After the considerable successes of third-generation ring-based light sources and the inauguration of linear-accelerator-based X-ray Free Electron Lasers (XFEL) [1,2], one of the main streams for future light sources is to develop a ring-based light source that can produce orders-of-magnitude higher brilliance than that generated by third generation light sources. With that goal in mind, newly designed storage rings for future light sources are based on multibend lattices with more than two bending magnets in each unit cell [3–9]. In addition, most of those projects do not rely merely on the increase in the number of bending magnets to obtain smaller emittance [10]; various dipole magnets with field gradients have been proposed and have played key roles in pushing the limit. A bending magnet with a transverse field gradient, which is equivalent to an off-axis quadrupole magnet, is expected to lower the emittance, taking advantage of its compactness and the availability of damping partition control. A bending magnet with a longitudinal field gradient, which we refer to hereinafter as a longitudinal gradient bend (LGB) is also expected as a new option to facilitate low emittance lattices [11]. In an LGB, electrons are bent by a large angle when a dispersion function is small and vice versa, thereby suppressing quantum excitation in electron bunches. Thus, the development of bending magnets with field gradients is one of the key issues for future accelerators.

*twatanabe@spring8.or.jp

At the SPring-8 third generation synchrotron radiation facility in Japan, a major upgrade (known as SPring-8-II) has been discussed that would target substantial improvements in light source performance [6]. For that purpose, a five-bend achromat lattice is being designed at an electron energy of 6 GeV [12]. In the new lattice, four out of the five bending magnets are LGBs, and the remaining one at the center of the unit cell is a normal bending magnet (NB). The resulting natural emittance of the bare lattice is estimated to be down around 150 pm · rad, and is expected to be reduced further to around 100 pm · rad by additional damping at the insertion devices. In addition to this low emittance, another underlying concept for the project is energy saving, both for achieving significantly better light source performance and for reducing power consumption. Another essential concept is related to stability and reliability. Because one of the strengths of a ring-based light source is its stability and reliability, we deem it important to maintain those strengths in the next generation light source. These concepts are taken into consideration throughout the design of SPring-8-II.

This is where permanent magnets come into play. Permanent magnets consume no energy in user operations [13], and there is no risk of power supply failure unless electricity has to be supplied for some specific reason. These features match the requirements for future accelerators, wherein stability and reliability are taken for granted. The absence of winding coils could also be beneficial if a new lattice is to be designed to have a high packing factor. The physical interference with an adjacent magnet, a beam position monitor and/or other components could be relaxed.

However, we suggest that there are practical challenges to using permanent magnets as the main magnets (e.g., dipole, quadrupole, and sextupole magnets) in future light

sources. Our claim is supported by the fact that no modern light sources use permanent magnet based main magnets. First, there is no straightforward way to readily tune the magnetic field, especially over a wide dynamic range. Second, the magnetic field generated by a permanent magnet is known to be temperature dependent [14,15], which affects the electron energy and lattice functions when the ambient temperature changes. Third, demagnetization of permanent magnets in undulators have been observed at several light sources [16–20], which should be avoided for the main magnets. Further, it is necessary to discuss the feasibility of producing the newly proposed bending magnets with field gradients as permanent magnet based main magnets for light sources.

In this paper, we discuss and summarize the issues that should be addressed in the design of permanent magnet based main magnets for future light sources, and we propose possible solutions. The proposed designs are tested and verified numerically and experimentally.

Although our main work is targeted mainly at developments for SPring-8-II [21–23], this paper presents a general discussion on the possibilities of using permanent magnets for future light sources and other accelerators. Other multipole magnets could be designed on a permanent magnet basis as well, but we here focus on the developments in dipole magnets.

II. DESIGN AND PERFORMANCE OF PERMANENT MAGNET-BASED DIPOLE MAGNETS

The main specifications for the SPring-8-II bending magnets are summarized in Table I. In an NB, the dipole magnetic field is homogeneous so that electrons experience a constant dipole field along the magnet except for edge fields. In the LGBs specified in Table I, the dipole field comes in a stepwise distribution with three different strengths, so electrons are bent with increasing or decreasing kick angles in a single magnet.

In the following, we address and discuss the main issues regarding the practical production of permanent magnet based dipole magnets.

TABLE I. Specifications of bending magnets for SPring-8-II (interim).

Magnet	NB[a]	LGB[b]
Maximum field (T)	0.95	0.79
Effective length (m)	0.42	1.75
Gap (mm)	25	25
GFR[c] (mm)	±6	±6
Magnets per cell	1	4
Magnets per ring	44	176

[a]Normal bending magnet.
[b]Longitudinal gradient bending magnet.
[c]Good field region where field deviation is within 0.1%.

A. Field adjustability

One of the key challenges with a permanent magnet is how to adjust its magnetic field. The main magnets of accelerators are often required to be tunable in precise and repeatable ways, for which electromagnets have played important roles. However, adjustable fields have been proposed and discussed for permanent magnets [24–31], especially for providing variable focusing fields.

Although not every case requires the magnetic field to be adjusted dynamically over a wide range, some amount of adjustability is required either to tune the magnetic fields precisely at the outset or to compensate for demagnetization later on. For our purposes, we have developed the adjustable-field dipole magnet that is illustrated in Fig. 1.

In nonadjustable magnets, the magnetic circuit is designed so that as much as possible of the magnetic flux generated by the permanent magnet goes into a closed loop through the beam axis [32]. In Fig. 1, a portion of the magnetic flux is intentionally leaked out of the closed loop by making other loops (dashed line). Thus, it becomes possible to change the magnetic flux density on the beam axis by mechanically moving the outer plates:

$$B_{\mathrm{gap}} = \frac{\phi_{\mathrm{gap}}}{S_{\mathrm{gap}}} = \frac{\phi_{\mathrm{pm}} - \phi_{\mathrm{loss}} - \phi_{\mathrm{op}}(\boldsymbol{r})}{S_{\mathrm{gap}}}. \quad (1)$$

Here B_{gap}, ϕ_{gap}, and S_{gap} are respectively the magnetic flux density, the magnetic flux, and the cross sectional area in the gap. The magnetic flux, ϕ_{pm}, is generated by permanent magnets. A difference between an electric circuit and a magnetic circuit is that the loss of flux, ϕ_{loss}, may not be negligible mainly because of the finite permeability of iron. Now, the part of the remaining flux, ϕ_{op}, that is intentionally leaked to the outer plates can be described as a function of the outer plate position, $\boldsymbol{r} = (x, y, z)$. The flux ϕ_{op} can be

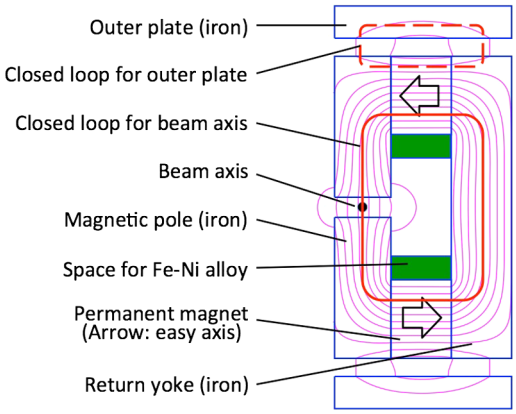

FIG. 1. A magnetic circuit for an adjustable-field C-shaped dipole magnet. The red solid curve represents a closed loop of the magnetic flux for the beam axis. The red dashed curve is for leaked flux. The arrows show easy axes of permanent magnet pieces. The green squares are spaces for Fe-Ni alloys (see Sec. II B).

estimated by numerical simulations, but in the Appendix we briefly discuss analytical expressions for the magnetic circuit assuming a simple model.

The proposed scheme has the following advantages. First, because the flux is varied mechanically, no electric power is necessary while the magnets are in use; even if the outer plates are moved electrically, the power supply can be turned off after the tuning. Hence, no malfunctioning of the dipole magnet due to a power supply failure is expected while it is in use. Second, given that the magnetic field need only be varied by a fraction of its full range, only a small portion of the magnetic flux needs to be leaked to the outer plates. Consequently, because magnetic force is proportional to the square of magnetic flux density, the mechanical force required to move the plates against the magnetic force can become significantly lower than that needed to vary the gap of the magnet. If the magnetic field is to be adjusted within 10% (i.e., 0.1), the necessary mechanical force is just 1% (i.e., 0.1^2) or less of that required to change the gap. This enables us to simplify the mechanical structure. Third, the magnetic field can be adjusted continuously and smoothly in a repeatable manner. This feature may open a possibility to turn the magnetic field almost off during maintenance works, then restore it to a nominal value prior to accelerator operation. In the Appendix, it is analytically shown for the simple model that the magnetic flux density in the gap can in principle be varied by 100%. The tuning range in practical cases is discussed in the following.

To assess the proposed scheme, we fabricated and tested a C-shaped dipole magnet with outer plates as shown in Fig. 2. The cross sectional view of the magnet is essentially that shown schematically in Fig. 1. The magnet consists of Neodynium-Iron-Boron (NdFeB) magnet (NMX-33UH, Hitachi Metals, Ltd.) and iron. Nonmagnetic materials such as aluminum alloy and stainless steels are also used for elements such as supporting frames and screws. The remanence B_r and the coercivity H_{cB} of the NdFeB magnet are 1.19 T and 930 kA/m, respectively. The gap is 25 mm with a pole width of 50 mm. The magnet pole length is 100 mm in longitudinal axis for the test case. Even if the magnetization in the NdFeB blocks are not perfectly homogeneous, the magnetic field distribution near the gap is smoothed out by the high permeability of iron ($\mu_r \sim 5000$). The outer plates are set at the bottom and on the top of the main magnet, and each are 80-mm thick. The plates are moved up and down manually in the case, although this could be done electrically and/or remotely, if necessary.

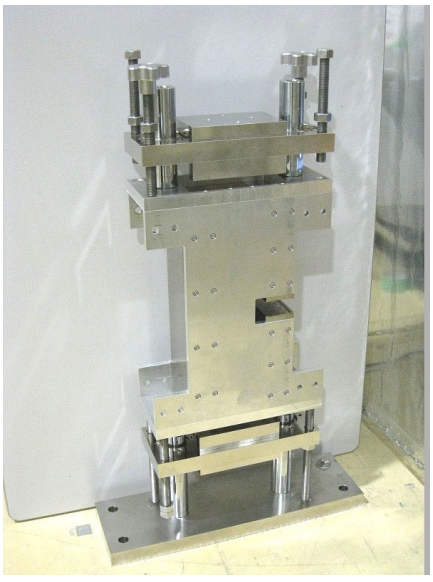

FIG. 2. C-shaped dipole magnet with outer plates.

The measured magnetic flux density in the gap as a function of the outer plate position are plotted with red circles in Fig. 3. Here the zero position corresponds to the outer plate touching the top or the bottom of the main magnet. For simplicity, the top and the bottom outer plates are set at the same distances from the main magnet in Fig. 3. We verified that the magnetic field could be varied smoothly over a wide range of 93.4%. It follows that approximately 6.6% of the full field remains in the gap mainly due to the finite permeability of outer plate irons. The achievable dynamic range depends on the detailed design of the magnet.

The analytical result obtained in the Appendix is also shown in Fig. 3. Here the normalized factors in the Appendix are assumed to be $B_0 = 0.118$ T and $L_n = 1.68$ mm to fit the analytical result to the measurement. Although more detailed modeling and/or numerical simulations are necessary for more precise comparison, it is analytically demonstrated as well that moving the outer plates can change the magnetic flux density in the gap.

Both the measurement and analytical results show that the slope of the magnetic field variation increases as the

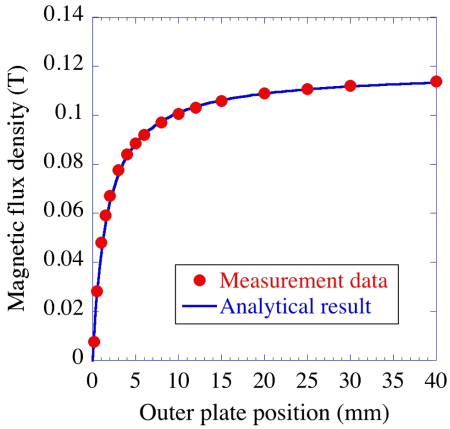

FIG. 3. Measured data (red circles) and analytical result (blue line) of magnetic flux density as a function of the outer plate position. See the Appendix for the analytical result.

outer plate is moved closer to the magnet pieces, and vice versa. In our case, we choose a magnetic field in the gap when the outer plate is set such that the slope of the magnetic field variation is small, for example at 25 mm in Fig. 3. Thus, the field across the gap changes by 0.3% on moving the outer plates by 1 mm at the position of 25 mm. Considering the typical precisions of the mechanical elements that move the outer plates, we expect that the outer plates can be adjusted precisely enough for most of our purposes.

B. Temperature dependence

The magnetic flux ϕ_{pm} generated by the permanent magnet changes with temperature as,

$$\phi_{\mathrm{pm}} = (1 + k_{\mathrm{pm}}\Delta T)\phi^0_{\mathrm{pm}}, \tag{2}$$

where k_{pm} is the temperature coefficient of the magnet and ϕ^0_{pm} represents the original magnetic flux before the temperature drift ΔT. The temperature coefficient k_{pm} is generally negative, that is, generated magnetic flux decreases as temperature increases. In Eq. (2), we assume simply that the temperature dependence is linear, which is practically acceptable within the operating temperature range of magnet. According to Eqs. (1) and (2), the magnetic flux density in the gap varies according to the temperature of the magnet.

One way to suppress the temperature dependence is to add another material with a different temperature coefficient to the magnetic circuit [33,34]. In this case, we added Fe-Ni alloy with a larger temperature coefficient than that of the permanent magnet. The places where Fe-Ni alloys are inserted in our case are shown in green squares in Fig 1. Part of the magnetic flux generated by the permanent magnet is shunted by the Fe-Ni alloys as follows:

$$\begin{aligned}\phi_{\mathrm{gap}} &= \phi_{\mathrm{pm}} - \phi_{\mathrm{sh}} \\ &= (1 + k_{\mathrm{pm}}\Delta T)\phi^0_{\mathrm{pm}} - (1 + k_{\mathrm{sh}}\Delta T)\phi^0_{\mathrm{sh}},\end{aligned} \tag{3}$$

where k_{sh} is the temperature coefficient of the shunt alloy, and ϕ^0_{sh} is the original flux passing through the alloy before the temperature drift. Here, the loss of flux ϕ_{loss} is omitted for simplicity. According to Eq. (3), the flux, and consequently the flux density, in the gap becomes independent of the magnet temperature when the second and the fourth terms on the right-hand side in Eq. (3) are cancelled with each other. The temperature coefficients for the permanent magnet k_{pm} and that for the shunt alloy k_{sh} are given on choosing the materials. The amount of flux generated by the permanent magnet, ϕ_{pm}, is determined by its volume and orientation. The flux in the shunt alloy, ϕ^0_{sh}, depends on the geometry of the magnetic circuit, such as the position and size of the shunt alloy. It follows that one only has to choose the right size and the place of the shunt alloy to adjust the magnetic flux ϕ^0_{sh} of the shunt circuit.

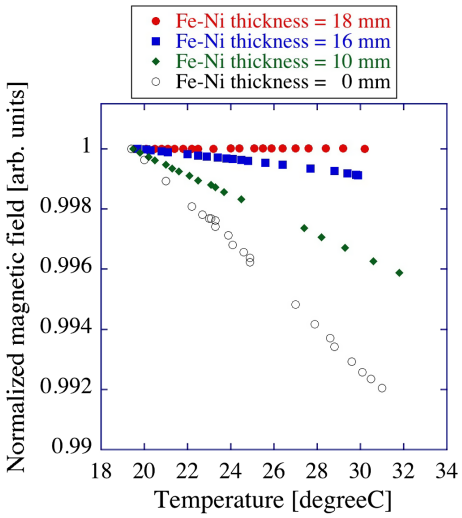

FIG. 4. Temperature dependence of magnetic field on beam axis for different thicknesses of Fe-Ni alloy.

We tested the scheme by using the same C-shaped dipole magnet with several sizes of Fe-Ni alloys (MS-2 [35]; Hitachi Metals Neomaterial, Ltd.) without outer plates. We used thermocouples to measure the temperatures on magnet surfaces, and nuclear magnetic resonance (NMR) probes to measure the magnetic fields. The open circles in Fig. 4 indicate the normalized magnetic flux density B in the gap without compensation. As expected, the magnetic flux density decreases as the temperature increases, and we estimate the temperature coefficient k_{pm} to be -7.0×10^{-4}. The temperature dependence lessens as the thickness of Fe-Ni alloy is increased. The temperature dependence has almost disappeared once the thickness reaches 18 mm, and the magnetic flux density in the gap no longer changes with temperature within the measurement accuracy.

The measured temperature coefficients for different alloy thicknesses are plotted in Fig. 5. The data are fitted linearly, because the flux in the shunt alloy is supposed to be linearly proportional to the thickness. In this case, it follows that the temperature dependence of the magnet is well compensated by choosing a thickness of 18 mm. We estimate from the fitted line in Fig. 5 that the residual temperature coefficient due to any imperfection in the alloy thickness is $4 \times 10^{-5}/°\mathrm{C}/\mathrm{mm}$, which gives a sense of how precisely the alloy thickness must be adjusted. If we require to stabilize the magnetic field within $10^{-4}/°\mathrm{C}$, we should adjust the alloy thickness to a precision of 2.5 mm, which is feasible with a general cutting machine.

C. Manipulation of magnetic field distribution

As described in Sec. I, one of the new features for next generation light sources is dipole magnets with transverse or longitudinal gradient. We have designed and fabricated

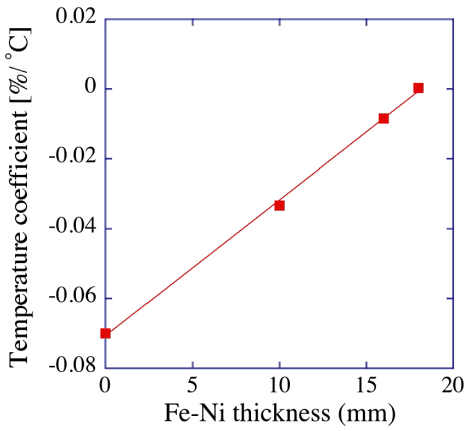

FIG. 5. Temperature coefficient versus shunt-alloy thickness. Squares are measured data. Solid line is a linearly fit to the measured data.

test dipole magnets with longitudinal field gradients, i.e., LGBs.

Table II summarizes the detailed parameters of the LGBs for SPring-8-II. The five bending magnets are numbered as BM1 to 5, and four out of the five (BM1, 2, 4, and 5) are LGBs. The magnet in the center of the cell, BM3, is a normal bending magnet without a field gradient. Each LGB consists of three segments, named A, B, and C, each of which generates a different field strength to form a step-functioned longitudinal field gradient. Because of the symmetry of the lattice, BM1 and 5, and BM2 and 4 are respectively identical but with opposite directions of the field gradient.

From the viewpoint of lattice calculations, the longitudinal magnetic field gradient does not necessarily have to be stepwise. Because the electron dispersion function varies continuously, the field variation should ideally be smooth and continuous. Such a field variation can be generated by a gradually varying gap or some alternatives [31]. In our case, the stepwise distribution is selected because it does not significantly increase the electron emittance compared with the ideal case. Such magnets are expected to have some advantages in manufacturing costs, field qualities, etc. by choosing a constant gap between segments. The benefits of the constant gap are discussed in the following.

TABLE II. Detailed parameters of LGBs for SPring-8-II. Each LGB is composed of three segments, named A, B, and C (interim).

Segments	L (m)	ρ (m)	B (T)
BM1A/BM5C	0.35	36.81	0.544
BM1B/BM5B	0.70	72.97	0.274
BM1C/BM5A	0.70	103.97	0.193
BM2A/BM4C	0.70	77.19	0.259
BM2B/BM4B	0.70	55.27	0.362
BM2C/BM4A	0.35	25.30	0.791

For producing the stepwise field distribution, it is intuitive to change gaps between segments as such. However, the edge field of a large gap segment extends over a long distance in the longitudinal axis, which is not preferable for SPring-8-II, and presumably other next generation light sources, where the packing factors are high. In addition, such a stepwise gap structure may cause undesirable field components including longitudinal fields. Also, a large gap requires more magnets, which requires more manufacturing costs. For the reasons, we choose a constant gap between segments, and the longitudinal field gradient is provided by different volumes of permanent magnets for each segment. Thus, the gap can be set to a minimum until it physically interferences with the vacuum components. By doing this, the edge fields from the LGB can be suppressed as low as possible. The leakage fields around the magnet is presented in Sec. II D.

For generating the longitudinal field gradient with the uniform gaps, different volumes of permanent magnet are needed for each segment. In addition, it is necessary to make a spacing between segments; otherwise, the field gradient is significantly reduced in the presence of high permeability irons ($\mu_r \sim 5000$). However, the spacings may yield dips in the longitudinal magnetic field distribution at segment boundaries. For this reason, we propose nose structures on the iron poles as illustrated in Fig. 6. Here, the segments have a longitudinal magnet length of 100 mm, and are separated by 30 mm. The nose structure sticks out of the pole edge by 7 mm each, so the distance between the nose edges is 16 mm. Numerical results simulated using the three-dimensional electromagnetic simulation code, CST Studio [36], and measurement result are compared in Fig. 7. Blue solid and dashed lines are simulated with and without the nose structures, respectively. Red open circles correspond to the measurement result. It is shown that the field gradient is well preserved by the spacings but field dips are found without the nose structures. Once the nose structures are added, the field dips are suitably

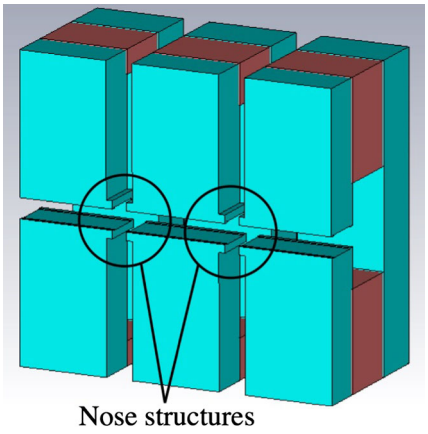

FIG. 6. Test longitudinal gradient bend (LGB) with nose structures.

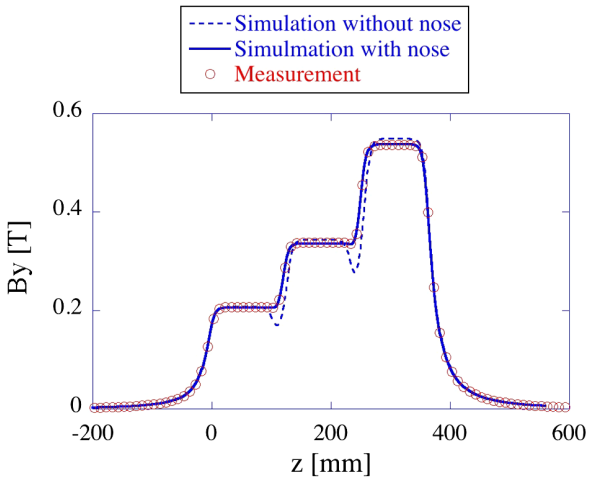

FIG. 7. Longitudinal field distributions with (blue, solid) and without (blue, dashed) nose structures by numerical simulations, and the measurement result (open circles).

eliminated. The measured longitudinal field distribution agrees well with the simulation result. Thus, it is verified that the nose structure is effective for producing a smooth transition of the magnetic field from one segment to the next while maintaining an adequate field gradient.

Another form of dipole magnet is one with a transverse gradient. There have been dipole electromagnets with transverse gradients in accelerators [3]. The fields are produced by a pair of facing poles shaped in a curve, or four poles like a quadrupole magnet but with a transverse offset against the beam axis [10]. Because the principle should hold true for permanent magnets as well, we assume it is feasible to produce such a transverse gradient with a permanent magnet.

D. Leakage field

Leakage magnetic fields around magnets need to be estimated for designing the magnets and accelerators. Because of the finite permeabilities of irons and permanent magnets, part of the magnetic flux leaks out of the magnet. It may be necessary to cover the magnet in nonmagnetic materials such as aluminum alloy and stainless steels to avoid unexpected accidents when the leakage fields are not negligible. For a high-packing-factor lattice, magnetic cross-talk between adjacent magnets may be evaluated prior to fixing the lattice.

The field distributions around the dipole magnet presented in Sec. II A are simulated by CST Studio as shown in Fig. 8. The calculation is performed without the outer plates for simulating the worst case concerning the leakage field. When the outer plates with enough thicknesses exist at the top and the bottom of the magnet as presented in Sec. II A, most of the leakage field near the top and the bottom of the magnet passes through the outer plates. The field distribution around the gap is similar to that for electromagnets

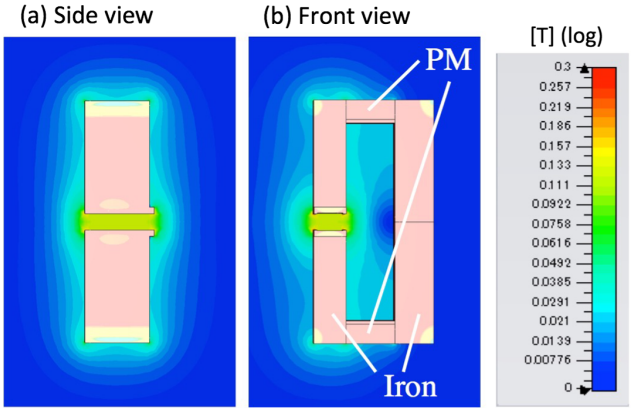

FIG. 8. Leakage field distribution around the dipole magnet on a log scale. High leakage areas are shown in red, while low leakage areas are in blue. PM stands for permanent magnet.

except for the field generated by winding coils. For suppressing the leakage field, one may add another permanent magnet that generates the reverse field of the leakage field, close the gap as discussed in Sec. II C, and/or insert magnetic shields around the magnet.

E. Demagnetization

A permanent magnet is demagnetized when radiation hits the magnet. Demagnetization of undulators has been observed because of the high radiation doses in accelerators, and the effects have been discussed at several accelerator facilities [14,16,18,37,38]. However, it should be emphasized that the conditions for the previous observations for undulators are different than those for dipole magnets in several aspects [39]. We shall discuss the differences between undulators and dipole magnets from the viewpoint of demagnetization in the following.

First, the permeance coefficient P_c, the ratio of magnetic flux density B and magnetic field strength H at the operation point, is different between undulators and dipole magnets:

$$P_c = -\frac{1}{\mu_0}\frac{B_d}{H_d}. \tag{4}$$

The permeance coefficients for undulators are typically a fraction of unity or even less because of their compact and complicated magnetic circuits, whereas dipole magnets can be designed so that the permeance coefficients are above unity. For instance, the estimated permeance coefficients of the C-shaped dipole magnet shown in Fig. 2 are averaged around four.

As far as the authors are aware, detailed mechanism of demagnetization due to radiation has not been fundamentally unveiled. Nevertheless, the mechanism has been well discussed based on the demagnetization curve, that is, the BH curve in the second quadrant, as a function of magnet

temperature. A strong correlation between the thermal behavior of magnets and the demagnetization due to radiation is observed experimentally [38]. As the magnet with the higher permeance coefficient is known to be less demagnetized in the high temperature circumstance, such a high-permeance-coefficient magnet tends to be less demagnetized due to radiation. Therefore, dipole magnets with high permeance coefficients are expected to be less demagnetized compared with typical undulators.

Second, our dipole magnets consist of iron and permanent magnets, and the magnet poles in the vicinity of the beam axis are made of iron. This structure is expected to prevent electrons from hitting the magnet pieces directly (see Fig. 1).

Third, most modern undulators are made of NdFeB magnet to take advantage of their high maximum energy product $(BH)_{\max}$. Instead, dipole magnets can afford to use Samarium-Cobalt except for those cases in which extremely high magnetic fields are mandatory. Because Samarium-Cobalt, particularly Sm_2Co_{17}, is known to have better characteristics than NdFeB in high temperature circumstances [10,14,15], it is expected that the demagnetization can be suppressed by choosing Sm_2Co_{17} [10]. Radiation damage studies, particularly comparisons between Samarium-Cobalt and NdFeB magnets, are underway.

III. CONCLUSION

Permanent magnet based bending magnets have been developed for future light sources. The main challenges are the field adjustability, the suppression of the temperature dependence of magnet, the demagnetization issue, and designing the variety of specific dipole magnets recently proposed for future accelerators. By introducing outer plates, shunt alloys with different temperature coefficients, and nose structures on iron poles, and by optimizing the design of the entire magnet, dipole magnets that are expected to be applicable to SPring-8-II magnets, and hopefully other future accelerators, have been designed, fabricated, and tested. As a result, both normal and longitudinal gradient bending magnets for SPring-8-II are being designed based on permanent magnets.

There are also possibilities for replacing other main magnets such as quadrupole and sextupole magnets with permanent magnets. In such cases, the feasibility of the field gradient adjustability is supposed to become one of the challenges. Yet, recent progresses in numerical simulation on nonlinear beam dynamics may change the design strategies of accelerators such that the magnet parameters are mostly fixed prior to constructing the accelerator. Should this be possible, the magnetic field gradients would not have to be tuned over a wide range, and small amount of tuning would have to be only provided by additional electromagnet correctors, or similar mechanisms as presented in the paper. There has been other work on the field adjustment of multipole magnets [24–31].

Further developments in the relevant research communities may open up new possibilities for constructing accelerators with significantly lower power consumption and failure rates.

ACKNOWLEDGMENTS

The authors are grateful to H. Tanaka and T. Ishikawa for support throughout the development of our magnet systems. We also wish to thank S. Sasaki, N. Kumagai, H. Kitamura, T. Tanaka, and T. Bizen for useful discussions on magnet design and the demagnetization effect. One of the authors (T. W.) would like to acknowledge J. Chavanne for fruitful discussions on magnets. This work was supported by the RIKEN SPring-8 Center (RSC) and by JSPS KAKENHI Grant No. 26600150.

APPENDIX ANALYTICAL EXPRESSIONS FOR THE MAGNETIC CIRCUIT WITH OUTER PLATES

For the magnetic circuit illustrated in Fig. 1, the magnetic reluctance in the gap, R_{gap}, is given by,

$$R_{\mathrm{gap}} = \frac{L_{\mathrm{gap}}}{\mu_0 S_{\mathrm{gap}}}, \tag{A1}$$

where L_{gap} and S_{gap} are the length and the cross sectional area, respectively, of the gap. In the same way, the magnetic reluctance between the main magnet and an outer plate is expressed by,

$$R_{\mathrm{op}} = 2\frac{L_{\mathrm{op}}}{\mu_0 S_{\mathrm{op}}}, \tag{A2}$$

where L_{op} is the length between the main magnet and the outer plate, and S_{op} is the cross sectional area of the outer plate facing the iron yokes of the main magnet. It is assumed here for simplicity that the magnetic flux does not go back and forth directly between permanent magnets and the outer plates. In Eq. (A2), the magnetic reluctance is multiplied by 2 because the magnetic flux passes through the air gap twice for a given gap length L_{op}. With two outer plates and two permanent magnets indicated in Fig. 1, the magnetomotive forces around the loop through the gap and that through the outer plate are written as,

$$2\phi_{\mathrm{pm}}R_{\mathrm{pm}} + \phi_{\mathrm{gap}}R_{\mathrm{gap}} = 0,$$
$$\phi_{\mathrm{pm}}R_{\mathrm{pm}} + \phi_{\mathrm{op}}R_{\mathrm{op}} = 0,$$

under the assumption of no significant losses in either the iron yokes or the plate. Thus, the magnetomotive forces for the gap and for the outer plates are related as,

$$\phi_{\mathrm{gap}} R_{\mathrm{gap}} = 2\phi_{\mathrm{op}} R_{\mathrm{op}} \tag{A3}$$

Now we recall Eq. (1) and assume for simplicity that the loss of the magnetic flux in iron yokes is negligible, then

$$B_{\mathrm{gap}} = \frac{\phi_{\mathrm{gap}}}{S_{\mathrm{gap}}} = \frac{\phi_{\mathrm{pm}} - \phi_{\mathrm{op}}}{S_{\mathrm{gap}}}. \tag{A4}$$

By substituting Eqs. (A1) (A2) (A3) into Eq. (A4), we obtain

$$B_{\mathrm{gap}} = \frac{\phi_{\mathrm{pm}}}{S_{\mathrm{gap}}} \frac{1}{1 + \frac{1}{4}\frac{L_{\mathrm{gap}}}{L_{\mathrm{op}}}\frac{S_{\mathrm{op}}}{S_{\mathrm{gap}}}}. \tag{A5}$$

According to Eq. (A5), when the outer plates touch the main magnet (i.e., $L_{\mathrm{op}} = 0$), the magnetic flux density in the gap goes to zero. When the outer plate is placed far away (i.e., $L_{\mathrm{op}} \to \infty$), the magnetic flux density in the gap becomes $\phi_{\mathrm{pm}}/S_{\mathrm{gap}}$ that corresponds to the one without the outer plates. The length L_{gap} and the cross sectional area S_{gap} of the gap, and the cross sectional area S_{op} of the outer plate facing the iron yokes of the main magnet are defined for each magnet setup. By introducing the normalizing factors $B_0 \equiv \frac{\phi_{\mathrm{pm}}}{S_{\mathrm{gap}}}$ and $L_n \equiv \frac{L_{\mathrm{gap}}}{4}\frac{S_{\mathrm{op}}}{S_{\mathrm{gap}}}$, Eq. (A5) is rewritten as,

$$B_{\mathrm{gap}} = B_0 \frac{1}{1 + \frac{L_n}{L_{\mathrm{op}}}}. \tag{A6}$$

The analytical expression in Eq. (A6) is plotted in Fig. 3 for the comparison with the measurement data. It is analytically demonstrated how the magnetic flux density in the gap can be adjusted by moving the outer plates.

[1] P. Emma *et al.*, First lasing and operation of an ångstrom-wavelength free-electron laser, Nat. Photonics **4**, 641 (2010).

[2] T. Ishikawa *et al.*, A compact X-ray free-electron laser emitting in the sub-ångström region, Nat. Photonics **6**, 540 (2012).

[3] M. Eriksson, L.-J. Lindgren, M. Sjöström, E. Wallén, L. Rivkin, and A. Streun, Some small-emittance light-source lattices with multi-bend achromats, Nucl. Instrum. Methods Phys. Res., Sect. A **587**, 221 (2008).

[4] L. Liu, F. H. de Sá, and X. R. Resende, in *Proceedings of the 7th International Particle Accelerator Conference, Busan, Korea* (JACoW, Geneva, 2016), p. 3413.

[5] P. Raimondi, ESRF-EBS: The extremely brilliance source project, Synchrotron Radiat. News **29**, 8 (2016).

[6] H. Tanaka, T. Ishikawa, S. Goto, S. Takano, T. Watanabe, and M. Yabashi, in *Proceedings of the 7th International Particle Accelerator Conference, Busan, Korea* (JACoW, Geneva, 2016), p. 2867.

[7] M. Borland, Preliminary expected performance characteristics of an APS multi-bend achromat lattice, https://www1.aps.anl.gov/files/download/Aps-Upgrade/multi-bend-achromat-lattice.pdf.

[8] H. Tarawneh, C. Steier, R. Falcone, D. Robin, H. Nishimura, C. Sun, and W. Wan, ALS-II, a potential soft X-ray, diffraction limited upgrade of the Advanced Light Source, J. Phys. Conf. Ser. **493**, 012020 (2014).

[9] R. Nagaoka, P. Brunelle, F. Cullinan, X.-N. Gvalda, A. Loulergue, A. Nadji, L. S. Nadolski, and M.-A. Tordeux, in *Proceedings of the 6th International Particle Accelerator Conference, Richmond, VA, USA* (JACoW, Geneva, 2015), p. 106.

[10] C. Benabderrahmane, J. C. Biasci, J. F. Bouteille, J. Chavanne, L. Farvacque, L. Goirand, G. Le Bec, S. M. Luizzo, P. Raimondi, and F. Villar, in *Proceedings of the 7th International Particle Accelerator Conference, Busan, Korea* (JACoW, Geneva, 2016), p. 1096.

[11] V. S. Kashikhin, M. Borland, G. Chlachidze, G. Decker, R. Dejus, J. DiMarco, C. L. Doose, T. J. Gardner, D. J. Harding, M. S. Jaski, J. S. Kerby, and A. V. Makarov, Longitudinal gradient dipole magnet prototype for APS at ANL, IEEE Trans. Appl. Supercond. **26**, 4002505 (2016).

[12] K. Soutome, K. Kaneki, Y. Shimosaki, M. Takao, and H. Tanaka, in *Proceedings of the 7th International Particle Accelerator Conference, Busan, Korea* (JACoW, Geneva, 2016), p. 3440.

[13] J. Citadini, P. P. Sanchez, R. Basilio, M. Rocha, E. W. de Siqueira, M. Potye, and G. Tosin, Sirius—a 3 GeV electron strorage ring based on permanent magnets, IEEE Trans. Appl. Supercond. **22**, 4004404 (2012).

[14] J. Chavanne and G. Le Bec, in *Proceedings of International Particle Accelerator Conference 2014, Dresden, Germany* (JACoW, Geneva, 2014), p. 968.

[15] D. Brandt, Report No. CERN-2010-004, 2009.

[16] T. Bizen, R. Kinjo, T. Hasegawa, A. Kagamihata, Y. Kida, T. Seike, T. Watanabe, T. Hara, T. Itoga, Y. Asano, and T. Tanaka, Radiation-induced magnetization reversal causing a large flux loss in undulator permanent magnets, Scientific reports **6**, 37937 (2016).

[17] M. Petra, P. K. Den Hartog, E. R. Moog, S. Sasaki, N. Sereno, and I. B. Vasserman, Radiation effects studies at the Advanced Photon Source, Nucl. Instrum. Methods Phys. Res., Sect. A **507**, 422 (2003).

[18] S. Sasaki, M. Petra, I. B. Vasserman, C. L. Doose, E. R. Moog, and N. V. Mokhov, in *Proceedings of the 21st Particle Accelerator Conference, Knoxville, TN, 2005* (IEEE, Piscataway, NJ, 2005), p. 4126.

[19] P. Colomp, T. Oddolaye, and P. Ellaeume, Report No. ESRF/MACH/93-09, 1993.

[20] H. Delsim-Hashemi, J. Roßbach, M. Tischer, A. Schöps, and Y. Holler, in *Proceedings of the 23rd Particle Accelerator Conference, Vancouver, Canada, 2009* (IEEE, Piscataway, NJ, 2009), p. 2423.

[21] T. Watanabe, K. Fukami, T. Nakanishi, and S. Sasaki, in *Proceedings of International Accelerator Conference 2014, Dresden, Germany* (JACoW, Geneva, 2014), p. 1253.

[22] T. Taniuchi, T. Aoki, K. Fukami, S. Takano, and T. Watanabe, in *Proceedings of International Particle*

Accelerator Conference 2015, Richmond, VA, USA (JACoW, Geneva, 2015), p. 2883.

[23] T. Watanabe, T. Aoki, H. Kimura, S. Takano, T. Taniuchi, K. Tsumaki, K. Fukami, S. Matsubara, C. Mitsuda, and T. Hara, in *Proceedings of International Particle Accelerator Conference 2016, Busan, Korea* (JACoW, Geneva, 2016), p. 1093.

[24] R. L. Gluckstern and R. F. Holsinger, Variable strength focussing with permanent magnet quadrupoles, Nucl. Instrum. Methods Phys. Res. **187**, 119 (1981).

[25] K. Halbach, B. Feinberg, M. I. Green, R. MacGill, J. Milburn, and J. Tanabe, Hybrid rare earth quadrupole drift tube magnets, IEEE Trans. Nucl. Sci. **32**, 3643 (1985).

[26] Y. Iwashita, Y. Tajima, M. Ichikawa, S. Nakamura, T. Ino, S. Muto, and H. M. Shimizu, Variable permanent magnet sextupole lens for focusing of pulsed cold neutrons, Nucl. Instrum. Methods Phys. Res., Sect. A **586**, 73 (2008).

[27] Y. Iwashita, M. Yamada, S. Ushijima, Y. Fuwa, Y. Nasu, H. Tongu, M. Masuzawa, and H. M. Shimizu, Variable permanent magnet multipoles, IEEE Trans. Appl. Supercond. **22**, 4000905 (2012).

[28] B. J. A. Shepherd, J. A. Clarke, N. A. Collomb, A. Bartalesi, and M. Modena, in *Proceedings of International Particle Accelerator Conference 2014, Dresden, Germany* (JACoW, Geneva, 2014), p. 1316.

[29] J. M. Krämer, A. Baurichter, M. Budde, F. Bødker, A. Irman, U. Lehnert, P. Michel, and U. Schramm, in *Proceeding of International Particle Accelerator Conference 2014, Dresden, Germany* (JACoW, Geneva, 2014), p. 2995.

[30] R. Gupta, Permanent magnet designs with large variations in field strength, IEEE Trans. Appl. Supercond. **14**, 473 (2004).

[31] Y. Arimoto, Y. Iwashita, T. Yoshioka, M. Kitaguchi, S. Imajo, H. M. Shimizu, K. Asahi, T. Ino, Y. Kamiya, K. Mishima, S. Muto, K. Sakai, T. Shima, K. Taketani, S. Yamashita, and A. Yoshimi, Development of longitudinal-gradient magnet for time focusing of ultracold neutron with anisotropic inter-pole, IEEE Trans. Appl. Supercond. **22**, 4500704 (2012).

[32] S. Russenschuck, Electromagnetic design of accelerator magnets, https://cds.cern.ch/record/941320/files/p411.pdf.

[33] J. T. Volk, Report No. FERMILAB-TM-2497-AD.

[34] K. Bertsche, J.-F. Ostiguy, and W. B. Foster, in *Proceedings of the Particle Accelerator Conference, Dallas, TX, 1995* (IEEE, New York, 1995), p. 1381.

[35] http://www.hitachi-metals-neomaterial.co.jp/english/product/liv/08.html.

[36] http://www.cst.com/.

[37] T. Bizen, T. Tanaka, Y. Asano, D. E. Kim, J. S. Bak, H. S. Lee, and H. Kitamura, Demagnetization of undulator magnets irradiated high energy electrons, Nucl. Instrum. Methods Phys. Res., Sect. A **467–468**, 185 (2001).

[38] A. B. Temnykh, Measurement of NdFeB permanent magnets demagnetization induced by high energy electron radiation, Nucl. Instrum. Methods Phys. Res., Sect. A **587**, 13 (2008).

[39] F. Bødker, L. O. Baandrup, N. Hauge, K. F. Laurberg, G. Nielsen, A. Baurichter, B. R. Nielsen, H. D. Thomsen, O. Balling, J. S. Nielsen, N. Hertel, S. P. Møller, F. B. Bendixen, P. Valler, and P. Kjeldsteen, in *Proceedings of International Particle Accelerator Conference 2014, Dresden, Germany* (JACoW, Geneva, 2014), p. 1226.